Research Article

Seungyeon Han#, Mohammad Shakhawat Hossain#, Taeho Ha, and Kyong Ku Yun*

Graphene-oxide-reinforced cement composites mechanical and microstructural characteristics at elevated temperatures

https://doi.org/10.1515/ntrev-2022-0495
received July 13, 2022; accepted September 14, 2022

Abstract: The focus of this research was to investigate the effects of graphene oxide (GO) on the microscopic composition, structure, pore size, and mechanical properties of GO-reinforced cement composites. Furthermore, the research explored the thermal behavior of GO-reinforced cement mortar at different elevated temperatures (250, 500, 750, and 1,000°C). This study considered three sets of GO-reinforced cement composites with 0.1, 0.2, and 0.3 wt% of GO (by weight of cement); the water–cement ratio in all the mixtures was 0.5. To characterize the chemical composition, microstructure, and hydration degree resulting from GO addition, X-ray diffraction, thermogravimetry, derivative thermogravimetry, scanning electron microscopy, energy-dispersive X-ray spectroscopy, and micro-computed tomography (Micro-CT) were used. The experimental results revealed that GO addition changed the microstructural composition and pore diameter distribution of the cement composite. The optimal amount of GO required for improving the mechanical properties of the cement composite under both unheated and heated conditions was identified to be 0.1 wt%. GO improves the cement matrices' ability to bind with GO nanosheets, leading to compressive strength retention and decreased micro-cracking (computed by material and defected volume changes by Micro-CT analysis). This is primarily due to the hydration products. However, the optimal amount of GO can result in nanomaterial agglomeration, thus lowering the thermal resistance of the cement composite. Overall, the study identified GO as a nano-additive with the potential to improve the strength and toughness of the cement composites. Moreover, the effect of elastic modulus was also evaluated. As a result, the GO microstructure analysis revealed that it has a porous structure with a visible crack pattern.

Keywords: cement nanocomposites, graphene oxide, microstructure, cement

1 Introduction

Cement is the fundamental binding material in concrete, but it is brittle and has low tensile strength. These disadvantages of cement were addressed by using steel and fiber reinforcements. Cement-based composites can be modified/re-engineered by incorporating small amounts of nanomaterials, leading to improved nanoscale properties of concrete, including toughness, durability, and flexural and tensile strengths [1]. Other researchers, on the other hand, investigated the extensive wear behavior of materials like SiC and B_4C-reinforced magnesium and aluminum alloy metal matrix composites. These included increased mechanical strength, durability, and microstructural integrity [2–4]. Moreover, Li *et al.* [5] studied the free-radical copolymerization of graphene oxide (GO) with methyl allyl polyoxyethylene ether, sodium styrene sulfonate, and acrylic acid resulting in GO-polycarboxylic acid superplasticizer (AA). Furthermore, supplementary cementitious materials with graphene nanoplatelet (GNP) of various concentrations from 0.025 to 0.10% by weight of cement are prepared to use a wet dispersion methodology which utilizes a high shear mixer and a polycarboxylate-based superplasticizer to dissipate GNPs in water [6]. Also,

# These authors contributed equally to this work and should be considered first co-authors.

*** Corresponding author: Kyong Ku Yun,** Department of Civil Engineering, Kangwon National University, 1 Gangwondaegil, Chuncheon, 24341, Korea, e-mail: kkyun@kangwon.ac.kr
Seungyeon Han: Korea Institute of Civil Engineering and Building Technology (KICT), 283 Goyang-daero, Daehwa-dong, Ilsanseo-gu, Goyang-si, Gyeonggi-do, Korea, e-mail: syhan@kict.re.kr
Mohammad Shakhawat Hossain: Department of Civil Engineering, Kangwon National University, 1 Gangwondaegil, Chuncheon, 24341, Korea, e-mail: shakhawat@kangwon.ac.kr
Taeho Ha: Department of Civil Engineering, Kangwon National University, 1 Gangwondaegil, Chuncheon, 24341, Korea, e-mail: gkxogh2810@kangwon.ac.kr

Mowlaei *et al.* [7] examined the effects of silica-coated GO nanohybrids on the effectiveness and mechanical and microstructural characteristics of ordinary Portland cement (OPC) paste composites and the findings show that the rational design of GO nanohybrids is an effective method for producing stronger and more reliable Portland cement composites. So, carbon nanotubes (CNTs), carbon nanofibers derived from graphene, and nanosilica are some of the well-known nanomaterials used to enhance the mechanical properties of cement composites. The popularity of nanomaterials in the concrete construction industry has increased due to the numerous benefits they provide, ranging from increased mechanical strength to nanolevel void filling. With advances in cement and nanomaterial chemistry, the uses of CNTs, graphene, GO, and graphene-based nanomaterials have improved the mechanical, thermal, electrical, optical, and other desirable properties of cement composites. Many researchers have reported improvements in the mechanical properties and durability of nano-reinforced cement composites compared with those of conventional cement composites [8,9].

In 1859, Brodie first synthesized GO, a carbon-based nanomaterial, by chemically exfoliating graphite (further modified by Hummer) [10]. GO, like graphite, has an aromatic structure, along with a large specific surface area (700–1,500 m^2/g) and a high aspect ratio (15,000–45,000). Zeng *et al.* [11] used two types of GO nanosheets as additives in this article to lessen the permeability of cement mortars. The results of the tests show that 0.06 wt% GO-1 (aspect ratio 50,000) and GO-2 (aspect ratio 5,000) reduce the relative permeability coefficient by 80.2 and 41.0%, respectively. In the case of 0.06 wt% dosage and normal arrangement, the relative permeability ratio is reduced by 80.6% if the aspect ratio is increased ten times. However, chemical reactions cleaved some of its covalent bonds, and functional groups like epoxy, carbonyl, hydroxyl, phenol, *etc.*, were attached to the sp^2 aromatic monolayer structure (about one atom thick) [12,13]. Among these functional groups, the oxygenated ones are hydrophilic in nature, allowing them to absorb free water radicals from the prepared cement composite, thus enabling easy dispersion in water; this overcomes the common disadvantage of the lack of dispersibility of nanomaterials. According to Chuah *et al.* [14], the GO dispersion in water was independent of the degree of sonication. Moreover, agglomeration occurred because the repellent forces provided by the oxygenated functional groups at GO sheets were overcome by the van der Waals forces between the GO nanosheets [15]. Because of its superior mechanical, thermal, and electrical properties, GO, a two-dimensional nanomaterial composed of flat monolayers of sp^2 carbon atoms, has piqued the interest of researchers since its discovery in 2004 [16]. Besides, a cluster of GO nanosheets provides a large surface area, which allows easy absorption of water molecules during wetting, and a bulky lateral size, which affords a high capacity for water retention; therefore, the addition of GO to cement-based composites has a negative impact on workability [17,18]. Regardless of the drawbacks of GO mentioned above, the incorporation of a small amount of GO (~1% by weight of cement (BWOC)) increased the compressive strength of hardened cement paste by 63% [19]. According to research [9,20], adding 0.05% GO (BWOC) increases the compressive strength of hardened cement paste by 15–33% and flexural strength by 41–58%. According to Shang *et al.* [21], the compressive strength of the cement paste with 0.04% GO (BWOC) increased by up to 15.1% when compared with that of the plain cement paste. On the inclusion of 0.03% GO (BWOC) in OPC paste, the compressive and tensile strength increased by ~40% after 28 days of curing [22]. In another study, Zhu *et al.* [23] found that incorporating 0.05 wt% of GO into cement mortar increased the compressive strength by 15–33% and tensile strength by 41–59%. According to Lv *et al.* [24,25], using GO in cement paste and mortar improved the mechanical properties. In addition, the analysis indicates that when the GO content is 0.05% under the same curing conditions and eons, the flexural strength of the test samples after curing for 28 days is the maximum, approaching 10.8 MPa, and the average percentage is 16.1%. The compressive strength of the samples after 28 days of curing is particularly high whenever the GO content is 0.03%, attaining 64.5 MPa, and the rate of development is 12.4%. Furthermore, when the GO dosage is 0.03%, the mortar's durability is greatly improved. The mortar has an impermeability that is 80% greater than the comparison samples [26]. Furthermore, GO in multiple various proportions by weight of cement are 0.01, 0.02, 0.03, and 0.04%. At 28 days of curing, experimental results revealed that cement composite specimens with 0.03% GO addition had 14.5, 30, and 40.47% relatively low water absorption capacity, chloride migration coefficient, and chloride penetration depth than normal cement composite specimens. Mechanical characteristics of cementitious composites were optimized by 77.70% in flexural strength at 0.03% GO addition and 47.61% in compressive strength at 0.04% GO addition after 28 days of curing [27]. Chen *et al.* [28] investigated the high-temperature properties of cement pastes containing GO agglomerates at 105, 200, 300, and 450°C. In general, incorporating GO can improve the thermal resistance of the cement paste by refining the pore structures and crystal sizes of calcium hydroxide ($Ca(OH)_2$; CH) at ambient

temperatures. The desirable microstructural and mechanical characteristics and durability of the cement-based composites are degraded at high temperatures [29,30]. As concrete constituents, cement and aggregates are not stable at high temperatures, and undergo physical and chemical transformations. The effects of temperature on the properties of cementitious composites, as well as the methods for preventing thermal degradation of concrete, have been described in several comprehensive reports [31–35]. Nanomaterials have recently gained prominence as potential admixtures capable of improving the properties of cementitious composites in both unheated and heated states [36–42]. The potential use of carbon-based nanomaterials, such as CNTs, GO, and graphene sulfonate nanosheets, for preventing the thermal degradation of cement-based composites has been studied [43–46].

Some researchers have observed that the GO inclusion accelerated the cement hydration. The oxygenated GO sheets attract the cement particles, allowing the nanosheets to act as nuclei for the cement phases, enhancing the hydration of cement [47]. Wang *et al.* reported that the microstructure of the GO-reinforced cement matrix had a large crystal structure covering, implying that CH leaching during the hydration stages was improved after 28 days of curing [48]. In addition, cement composites have high compressive strengths but low tensile and flexural strengths due to their brittleness, which results primarily from the hydration products like CH, calcium silicate hydrate (C–S–H) gel, ettringite (AFt), and monosulfonate (AFm) in the hardened cement paste. CH, AFt, and AFm are examples of hydration crystals that typically have rod-like and needle-like shapes [49]. As an example, through the use of dispersant and ultrasonic pre-dispersion, the current study successfully develops a new method for preparing rGO suspension with excellent dispersibility and stability. At 3 days, the compressive and flexural strength of the mortar had already enhanced by 45 and 50%, respectively. In the meantime, the hydration heat and pore structure have continued to improve to a doping concentration of 2.00 wt% rGO [50]. GO was found to improve the toughness of cement mortar by modifying the microstructure. Moreover, significant improvement in the mechanical properties of cement resulted from improved GO dispersion due to the interlock mechanism of C–S–H (bridging by chemical bonding) [51]. Anhydrous cement is composed of Bogue's compounds, such as tricalcium silicate (C_3S, Ca_3SiO_5), dicalcium silicate (C_2S, Ca_2SiO_4), tricalcium aluminate (C_3A, $Ca_3Al_2O_6$), tetracalcium aluminoferrite (C_4AF, $Ca_4Al_nFe_{2-n}O_7$), and small amounts of gypsum (Na_2SO_4, Ka_2SO_4). These compounds will undergo hydration to form AFt ($Ca_6Al_2(SO_4)_3(OH)_{12}{\cdot}26H_2O$), AFm ($Ca_4Al_2(OH)_2{\cdot}SO_4{\cdot}H_2O$), CH, and C–S–H gel ($3CaO{\cdot}2SiO_2{\cdot}4H_2O$) [25]. The brittleness of cement paste can be studied by observing the formation of rod-like and needle-like shaped crystals of CH, AFt, and AFm. The surface of GO contains numerous oxygenated functional groups, primarily –OH, –COOH, and $–SO_3H$. The effective active groups on the surface of GO react with C_3S, C_2S, and C_3A to form the growth points for the hydration product. At the beginning of the hydration reaction, GO forms neighboring rod-like crystals on its surface, resulting in thick flower-like crystals. These flower-like crystals form a cross-linking structure between the gaps of cement composites, increasing the toughness of the cement composites [24]. GO is a layered nanomaterial composed of oxygenated graphene sheets with hydroxyl and epoxide functional groups on their basal planes and carbonyl and carboxyl groups on the sheet edges [52]. Typically, these oxygenated functional groups facilitate the dispersion of GO in water as 1 nm thick sheets [53]. The elastic modulus of the GO nanomaterial is ~32 GPa [18,54].

Some researchers have reported limited GO dispersion in cement composites. In cement-based materials, the dispersion of GO is crucial for improving compressive strength. The divalent calcium ions in fresh cement paste hinder the GO dispersion, which could adversely affect the GO performance in cement composites. Hunain [55] conducted a molecular dynamics analysis and found that the interfacial strengths between C–S–H gel and pristine, hydroxyl-functionalized, amine-functionalized, and carboxyl-functionalized graphene nanoplatelets and C–S–H reached 1.2, 13.5, 6.1, and 11.8 GPa, respectively. This suggests that the functional groups in the graphene nanoplatelets may improve the interfacial strength, mechanical properties, and toughness of the cement-based nanocomposites. Fan [56] reported that the use of graphene and GO in cement paste improved both the mechanical strength and Young's modulus. Babak *et al.* [57] discovered that adding 1.5 wt% of GO to cement mortar increased its tensile strength by 48% and that the most important hydration product is C–S–H gel. Liu *et al.* [58–60] discovered that C–S–H assumes the shape of a regular flower due to the nucleation and regulation of graphene (G)/GO during C–S–H formation. However, based on classical nucleation theory, Kong *et al.* [61] found no C–S–H on the surface of nanomaterials and concluded that the nanoparticles have no nucleation effect. The effects of G/GO on cement hydration remain unknown. The above-mentioned studies concentrated more on the morphology of C–S–H and less on the effect of G/GO on the C–S–H formation process.

To investigate the effects of GO additives in OPC, three sets of GO-reinforced composites (0.1, 0.2, and 0.3 wt%) were considered in this study. X-ray diffraction

Table 1: Chemical composition and physical properties of OPC

	Chemical composition						Physical properties	
	SiO_2	Al_2O_3	Fe_2O_3	CaO	MgO	SO_3	Specific area (cm^2/g)	Density (g/cm^3)
OPC	20.8	6.3	3.2	61.2	3.3	2.3	3,300	3.15

(XRD) analysis, thermogravimetry (TG), and micro-computed tomography (Micro-CT) were used to investigate the effects of GO on the microscopic composition, structure, pore size, and mechanical characteristics of the GO-reinforced cement composites. Furthermore, the thermal behavior of the specimens upon exposure to various elevated temperatures (250, 500, 750, and 1,000°C) was explored, which is a significant contribution and originality to our study.

2 Experimental details

2.1 Materials

Table 1 presents the chemical composition and physical properties of the OPC (Sungshin Portland Cement, Korea) used in this study. The GO obtained was brown in color (dark brown liquid solution), with a concentration in the range of 0.8–1.2 wt% (determined by a moisture titrator), pH 2–3, and conductivity of 2,000–4,000 μS/cm; the particle size range is 3–19 μm and the particle size at 50% in the cumulative particle size distribution (D50) is 8 μm. The thickness of GO, as determined by atomic force microscopy, is 1–1.2 nm. Figure 1 shows the scanning electron microscopy (SEM) particle size images, and Figure 2 shows the intensity of D and G bands obtained by Raman spectroscopy. Here, the G band results from in-plane vibrations of sp^2 bonded carbon atoms, whereas the D band results from out-of-plane vibrations due to structural defects. Moreover, GO was made with 1% of solution with a total weight of water and it was bought from the company Standard Graphene.

2.2 Composition of mixtures and sample preparation

Cement paste samples were prepared to determine the microstructure of the mixtures; mortar was prepared using OPC and OPC-composites with 0.1, 0.2, and 0.3% GO (BWOC) to determine the mechanical properties. The compositions of the various mixtures are given in Table 2. The cement-to-sand ratio was 1:3 in all the mixtures. The water-to-cement ratio (w/c) in the mortar was 0.5. The sample was collected for microstructure analysis after mixing. For the compressive strength and thermal heating measurements, molds of dimensions 50 mm × 50 mm were prepared. Micro-CT analysis was performed on specimens of dimensions 30 mm × 30 mm because the low-energy X-rays in micro-CT cannot penetrate thicker materials, whereas the high-energy X-rays cannot provide low-contrast information. The microstructure and properties were investigated using micro-CT. Cylindrical molds were

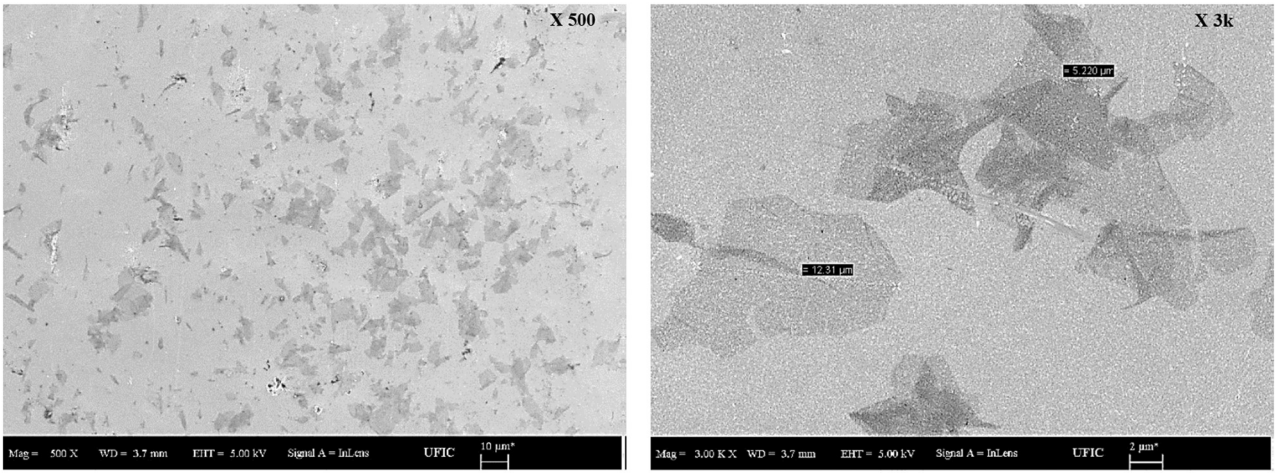

Figure 1: SEM particle size images.

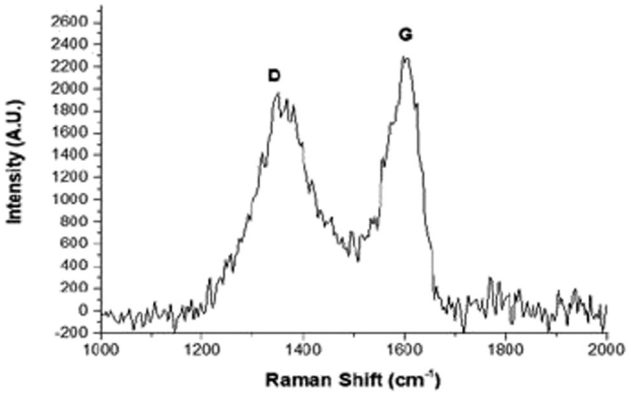

Figure 2: Raman spectroscopy image.

Table 2: Mix compositions for the experiments

Type	Water (g)	Cement (g)	Sand (g)	GO (wt%)
OPC	225	450	1,350	0
GO-0.1	225	450	1,350	0.1
GO-0.2	225	450	1,350	0.2
GO-0.3	225	450	1,350	0.3

prepared for measuring Young's modulus. For each age, the XRD and TG samples were solvent-exchanged with isopropanol and stored in a vacuum at room temperature (20 ± 3°C) for 1 day.

2.3 Testing and characterization

2.3.1 XRD

X'Pert PRO MPD X-ray diffractometer with CuKα target radiation was used to obtain the XRD patterns of the GO specimens. The specimens were continuously scanned over the diffraction angle (2θ) range of 5–70° at a scanning speed of 2°/min, with a step size of 0.002°.

2.3.2 TG and derivative thermogravimetry (DTG) analysis

TG and DTG analysis are done by different scanning calorimeter (DSC Q2000) and the features are heating flow = 20 °C/min to 1,050°C and N2 = 100 mL/min and heat flow.

2.3.3 SEM/energy-dispersive X-ray spectroscopy

For SEM analysis, the microstructure of the GO-reinforced cement paste samples were observed using the field emission scanning electron microscope (Hitachi SU8000, Japan).

2.3.4 Cement paste compressive strength at elevated temperatures

After 1, 7, 28, and 56 days of curing, the compressive strengths of the specimens cured at ambient temperature (20 ± 3°C) were evaluated. To eliminate water from the test samples for high-temperature tests, the samples were removed from the control room and oven-dried for 24 h prior to heating. Following this, the specimens were thermally treated in a furnace at a high temperature for 28 days. The specimens were then heated for 1 h at 1°C/min to temperatures of 250, 500, 750, and 1,000°C, followed by cooling at a rate of ~1°C/min to the room temperature (20 ± 3°C). To evaluate the compressive strength of the cement pastes, two cubic specimens were considered for each temperature.

2.3.5 Micro-CT to analyze cracking

The micro-CT equipment model was NIKON METROLOGY (XT H 225). The specifications of this equipment were maximum (max.) potential = 225 kV, X-ray spot size = 3 µm, max. sample dimensions = ~100 mm × 100 mm, and max. sample weight = 15 kg. Micro-CT was used to evaluate the thermal resistance of the cement pastes. Micro-CT is a noninvasive and nondestructive method for investigating the inner structures of the target materials, including cementitious materials [62,63]. Micro-CT is generally used to examine specific material aspects such as pores [64–66] or the presence of hydration products [67,68], while it has been used in some studies to analyze crack propagation [69–71]. Thus, micro-CT is a useful technique to investigate the mechanical behavior of cementitious materials.

2.3.6 Dynamic Young's modulus measurement equipment

Figure 3 shows the dynamic Young's modulus measurement equipment. The equipment specifications are as follows: power supply: AC 90–240 V (50/60 Hz); frequency range: 500–25,000 Hz; seven-stage switching; frequency and data display: five decimal digit precision; transparent blue liquid-crystal display of dimensions 54:32 mm; measurement waveform/analog meter display: a thin-film-transistor liquid-crystal color display of dimensions 86 mm × 30 mm; measurement range: longitudinal vibration, flexural vibration, and torsional vibration; measurement method: manual/automatic; vibration terminal: lead zirconate titanate;

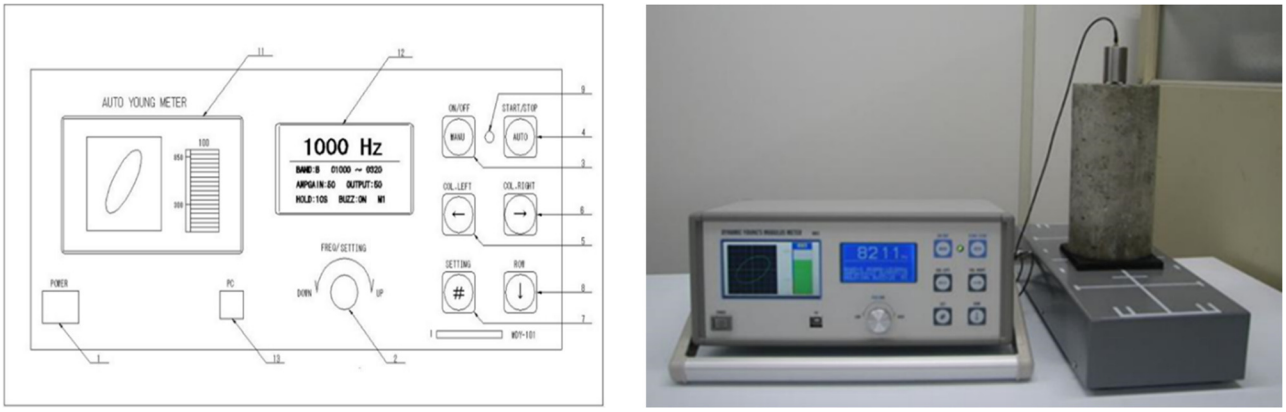

Figure 3: Dynamic Young's modulus equipment.

pickup: high sensitivity, lead zirconate titanate; external terminal: Universal Serial Bus connection for a computer with serial data output; body dimensions: 320 mm (width) × 133 mm (height) × 230 mm (depth); shaking table dimensions: 410 mm (width) × 60 mm (height) × 160 mm (depth).

3 Results and discussion

3.1 Workability

The mechanical characteristics and durability of hardened cement composites were found to improve with the increasing workability of cement pastes. Flow tests were conducted to investigate workability by assessing the flow and consolidation of a fresh cement composite mix. The results of the flow tests are shown in Figure 4.

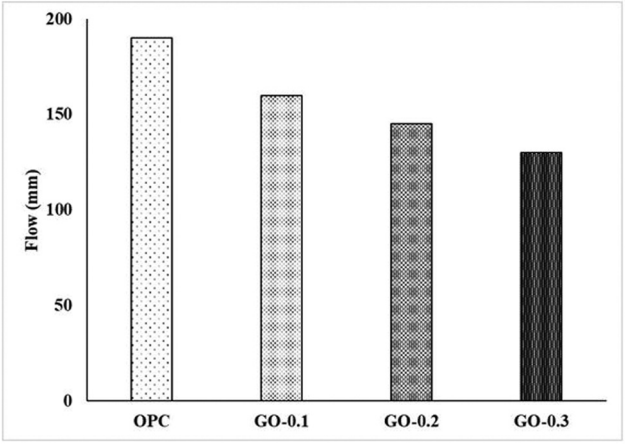

Figure 4: Flow test values of all samples.

Insufficient workability can complicate the compaction of a fresh cement composite and result in air void entrapment, which degrades the mechanical characteristics of cement composites [10,72]. Many researchers have reported that the addition of GO diminishes the workability of the cement composite. Because of its hydrophilic functional groups and large surface area, GO can absorb a large amount of water. Consequently, the quantity of water available to lubricate the cement particles decreases while the friction resistance between the cement grains increases [22,73–75]. Although a well-dispersed GO is desirable, with its higher specific surface area, the extra free water associated with the GO sheets reduces the workability of the cement composite; this is a major drawback of the GO-reinforced cement composite [21]. Some researchers have reported that the configuration of GO aggregates entrapped free water, significantly lowers the workability of cement composites [76,77]. Furthermore, because van der Waals forces between the GO sheets attract the cement grains, the physical interaction between GO and cement grains contributes to the reduced workability of the fresh cement composites [59,78].

3.2 Microstructural analysis of GO cement paste

3.2.1 XRD analysis of experimental samples

The XRD patterns shown in Figure 5 are used to characterize the crystalline phases to assess the hydration reactions that are taking place, as well as the degree of hydration. The XRD patterns of cement composites containing GO and the reference sample show no difference in crystallinity between them, indicating that GO addition does not affect

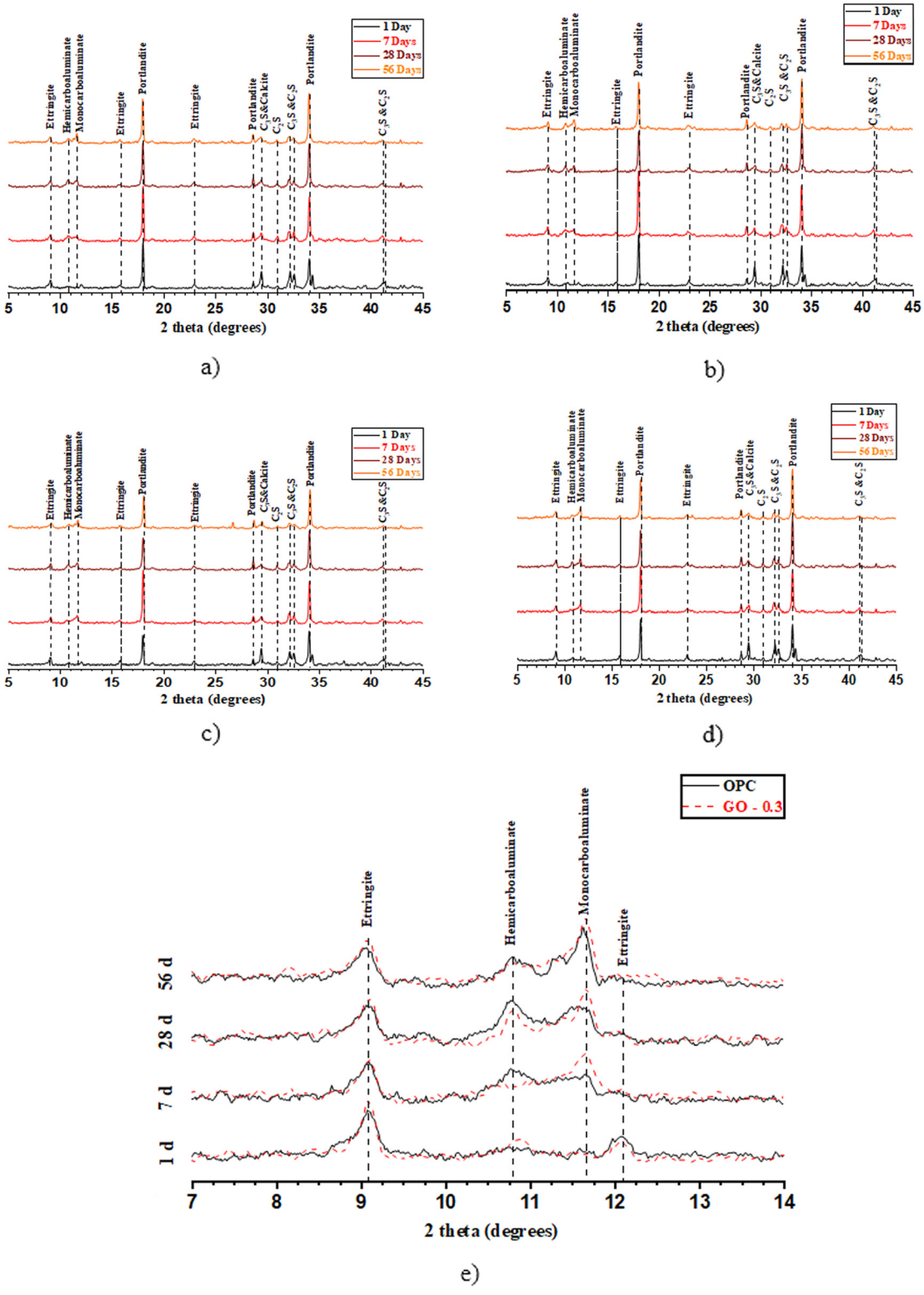

Figure 5: XRD patterns of OPC and GO-incorporated cement paste: (a) OPC, (b) GO-0.1, (c) GO-0.2, (d) GO-0.3, and (e) OPC and GO-0.3 specimens 2 theta (7–14°).

the crystal phases of the cement matrix [79–81]. The XRD patterns obtained in some studies revealed that with GO incorporation, the intensities of the peaks for cement components (alite and belite) decreased, while those for CH increased, indicating improved cement hydration in the presence of GO [82]. The evolution of crystals in composites is usually characterized by XRD analysis, with the diffraction peaks ranging from $2\theta = 5°$ to $2\theta = 45°$. The evolution of crystals has a direct impact on the microstructure and mechanical properties of OPC, GO-0.1, GO-0.2, and GO-0.3 after 1, 7, 28, and 56 days of curing. Alite, belite, AFt, monosulfoaluminate, AFm, hemicarboaluminate (H_C), and monocarboaluminate (M_C) were the major crystalline phases in anhydrous OPC. Calcite ($CaCO_3$) was also found in the OPC. The increase in interplanar spacing indicates that oxygenated functional groups are inserted into the carbon atomic layers following graphite oxidation. The covalent interaction between oxygen and graphite changes the structure of the graphene sheets, causing the GO diffraction peaks to shift.

Peaks corresponding to H_C were found in the range of $2\theta = 10–12°$ in all GO-incorporated samples (GO-0.1, GO-0.2, and GO-0.3) on the first day of hydration, which is the early stage of hydration, and no peak values were found in the OPC samples. With aging, H_C was gradually converted to M_C, and after 7 days, the M_C peak of the GO-incorporated sample reverted to the H_C peak within the same diffraction angle range (10–12°), indicating an aspect different from the OPC sample. Even after prolonged hydration and in the presence of calcium carbonate, H_C was found in the hydrated cement paste, despite the fact that M_C was expected to be thermodynamically more stable. Previous studies revealed that the conversion of H_C to M_C changes with time; in contrast, the H_C reflex values increased in all the samples after 28 days of aging. There was no difference in the H_C and M_C reflex values between the OPC samples and GO-incorporated samples after 56 days of aging. The incorporation of GO affects the H_C generation and is supposed to hasten the transition to M_C. Furthermore, with aging, the intensity of the AFt peak ($2\theta = 15–25°$) decreased when compared to that of day 1, because AFt transforms to monosulfoaluminate and then returns to the M_C or H_C phase. However, it is clear that the addition of GO promotes the formation of M_C and H_C, because the OPC samples are also subjected to the same process as described above during aging. In all the samples, with the increase of age, the clinker peaks ($2\theta = 25–35°$) of C3S and C2S decreased, while the peaks of AFt and AFm increased. There was no discernible peak difference for CH, a general hydration product. Because of the low contents of the added GO, no peaks corresponding to GO were found in the resulting XRD patterns. As a result, no significant differences in the diffraction patterns of different samples were observed, indicating that their mineralogical compositions were similar. The increased peak intensities were due to the accelerated cement hydration caused by the addition of GO.

3.2.2 TG analysis

Figure 6 shows the TG results for samples cured for 1, 7, 28, and 56 days. The weight loss for the GO-incorporated samples was higher than that of the OPC samples during 28 days of curing, indicating that additional hydration products resulted when GO was included as the additive. After 56 days of curing, there was no difference in weight loss between the OPC and GO-incorporated samples. This suggests that the inclusion of GO resulted in rapid hydration based on the initial nucleation, while the number of hydration products for the OPC and GO mixture was similar during long-term aging. The DTG curves of all the samples (Figure 6) showed weight losses below 200°C due to the evaporation of free and physically bound water and dehydration of C–S–H and AFt. The dehydration of the carbonated AFm phases, such as M_C and H_C, occurred at temperatures of ~150°C. The weight loss at temperatures ~360°C was attributed to siliceous hydrogarnet dehydration [83]. The peaks centered at 420 and 740°C were associated with portlandite dehydroxylation and calcite carbonation, respectively.

In TG analysis, the peaks of AFt and AFm generated at the early stage of hydration were observed to identify the accelerated cement hydration caused by the addition of GO. As in the XRD analysis, the peaks of the GO-incorporated sample were higher than those of the OPC sample on the first day of aging, which is the initial period of hydration. The disparity increased with aging. Furthermore, the carbonate peaks of GO-incorporated samples after 1 and 7 days were less intense than those of the OPC sample, indicating that monosulfoaluminate transformed into H_C or M_C with the inclusion of GO. This aligns with the result of the XRD analysis. Furthermore, in the cases of aging for 28 and 56 days, the differences in the values for all the samples are insignificant, which is thought to be due to the production of larger amounts of hydration products in the initial stage of hydration in the GO mix compared with OPC, while during long-term aging, the amounts of hydration products are similar in both. The quasi-water and CH contents of the cement pastes decided by the TG curves were used to evaluate the degree of cement hydration. Three prominent mass

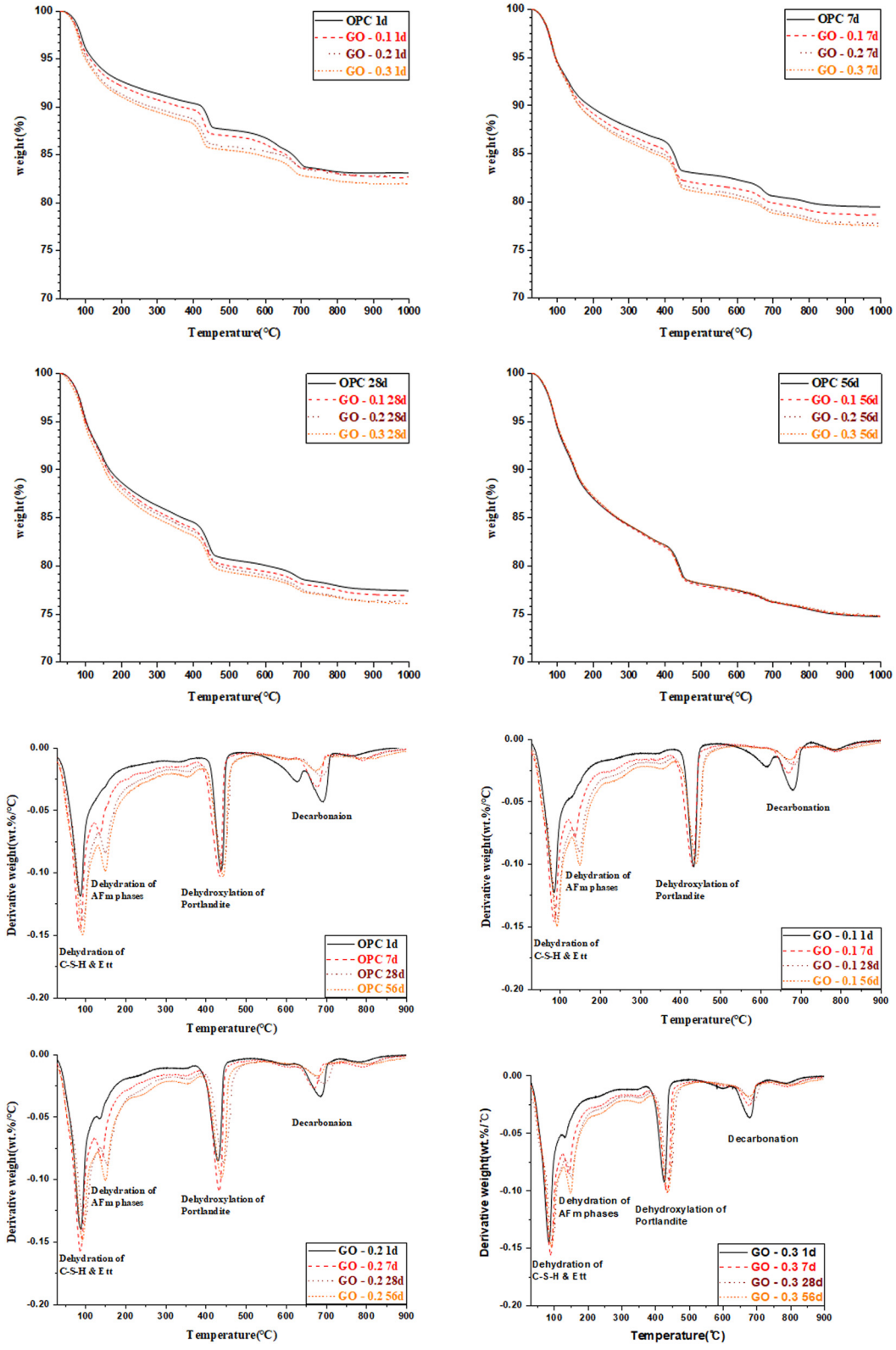

Figure 6: TG results for the samples.

failures can be identified in the temperature ranges of 120–150, 400–500, and 600–800°C, corresponding to the decomposition of C–S–H and AFt, CH, and $CaCO_3$, respectively, due to the unexpected carbonation [84–87].

3.3 Cement paste compressive strength before and after heating

Figure 7 depicts the compressive strength of cement pastes after 1, 7, 28, and 56 days of curing in atmospheric temperature (~20 ± 3°C). The incorporation of GO (0.1, 0.2, 0.3 wt%) had a noticeable impact on the mechanical properties of the cement paste. After 28 days, the specimen with ultimate compressive strength of 54.94 MPa was attained with the GO-0.1 paste. The compressive strength increased by 2.14, 24.58, and 17.24% for GO-0.1, GO-0.2, and GO-0.3, respectively, compared with that of OPC after 1 day. The compressive strengths of GO-0.1, GO-0.2, and GO-0.3 increased by 9.98, 19.34, and 18.12%, respectively, compared with that of the OPC sample after 7 days. After 28 days, the compressive strengths of GO-0.1, GO-0.2, and GO-0.3 increased by 6.78, 5.18, and 0.72%, respectively, compared with that of OPC. The significant increase in the compressive strength of the GO-reinforced cement composite can be attributed to porosity reduction (resulting in a compact microstructure) and GO's potential to bridge microcracks. The compressive strength of the GO blended specimens enhanced within the range reported in the literature. Devi *et al.* [88] discovered that integrating GO enhanced the compressive strength by 21–55%. Other studies have reported compressive strength enhancements ranging from 10 to 60%, depending on whether paste, mortar, or concrete is evaluated [89,90]. Furthermore, the compressive strength of the GO-0.1, GO-0.2, and GO-0.3 specimens after 56 days was higher by 2.33, 1.37, and 1.92%, respectively, compared with that of the OPC specimen. The effect of graphene on mechanical properties of the cement composite is highly dependent on the type and amount of graphene, and the extent of graphene dispersion in the cement matrix [91]. Here, it is observed that the inclusion of GO resulted in a minor increase in the compressive strength of the cement composite. The functionalization of the GO surface increases the cohesion between the GO nanosheets and the cement matrix's C–S–H, which enhances stress percolation and thus the mechanical performance of the samples [92]. This demonstrates that for GO-0.1, GO-0.2, and GO-0.3, GO was effectively dispersed in the cement matrix, resulting in higher strength. Despite the inclusion of an adequate amount of GO, GO clustering can weaken the bonding between GO and cement matrix and limit the enhancement of compressive strength with GO addition.

Figure 9 shows the results of calculating the relative remnant of compressive strength to successfully assess

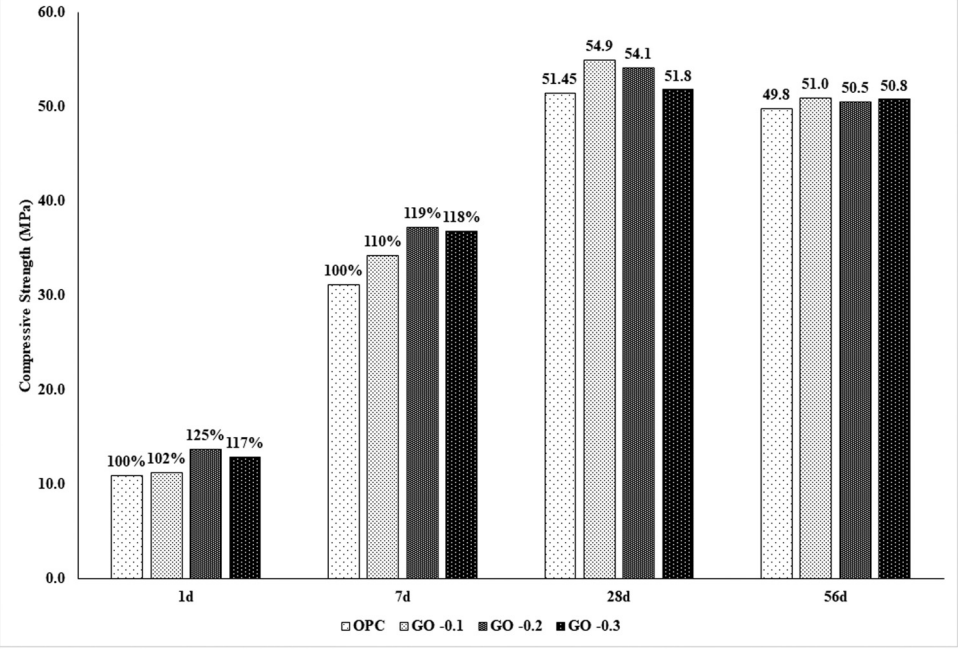

Figure 7: Compressive strengths of all samples.

the influence of temperature on the performance of cement pastes. These values were measured as the percentage increase/decrease in cement paste's compressive strength over time compared to the compressive strength of the unheated specimen (20 ± 3°C). The compressive strength of the 28-day GO-0.1 specimen was enhanced by 13.91% after exposure to 250°C; in contrast, the corresponding values of GO-0.2 and GO-0.3 were reduced by 5.57 and 7.44%, respectively, as shown in Figure 8. The strength of plain cement paste (OPC) deteriorated the least. Nevertheless, for the unheated samples, compared with the OPC specimens, the GO samples exhibited a significant improvement in compressive strength (13.91% enhancement for GO-0.1). GO-0.1 had the highest compressive strength (54.94 MPa) among all the specimens under unheated conditions. Furthermore, after exposure to elevated temperatures, GO-0.1 demonstrated excellent compressive strength. At elevated temperatures, the strength enhances due to additional hydration of anhydrous cement grains (as a result of an internal autoclaving reaction); furthermore, the additional hydration products fill the pores enhancing the compressive strength [46,93]. It is reasonable to conclude that the incorporation of 0.1 wt% of GO contributes to microstructure densification and compaction and that the creation of a less permeable microstructure allows for an increase in the effects of the autoclaving reaction. This impact is prominent when adequate amount of GO has been used. After exposure to 500°C, the compressive strength remained nearly identical to those after exposure to 250°C; however, the compressive strengths of GO-0.1, GO-0.2, and GO-0.3 were increased by 12.4, 1.62, and 0.51%, respectively, compared with that of OPC. A temperature of 500°C is generally considered harmful for cementitious composites due to the decomposition of C–S–H gel and CH, resulting in noticeable cracking in the specimens. However, when the specimens are not exposed to moisture for an extended period, this effect does not seem to be critical for their strength (re-hydration of lime to CH is limited) [94]; Heikal [95] and Kang *et al.* [96] reported significant enhancements in the compressive strength of cement paste after exposure to 400 and 450°C. Identical findings in the case of concrete have been reported by Hachemi and Ounis [97]. As a result of self-autoclaving, the anhydrous cement particles were further hydrated when exposed to 400°C [95]. Compared with OPC, the enhancement in strength was observed only in GO-1 after exposure to 500°C, and drastic reductions in strength was observed for GO.02 (10.26%) and GO-0.3 (8.68%) specimens at 750°C. For GO-0.1, the mentioned enhancement in strength is due to the improved bonding between cement matrices and GO nanosheets. In addition, the GO calcination resulted after 450°C, whereas the samples were shielded from calcination due to the presence of GO. These findings

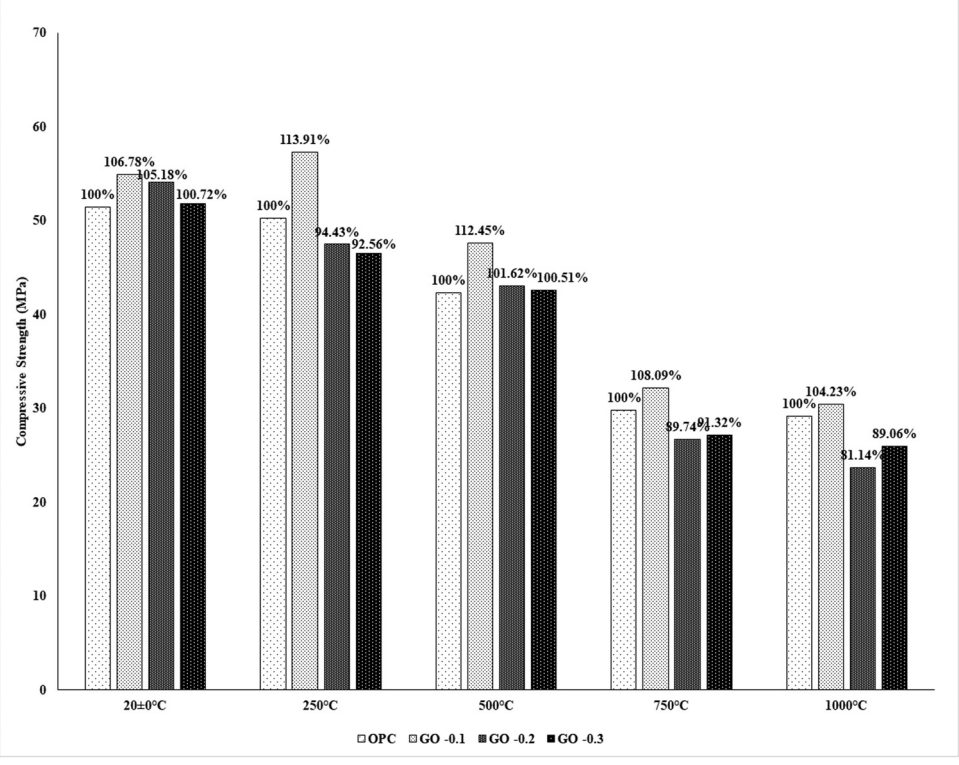

Figure 8: Compressive strengths of all samples after thermal exposure.

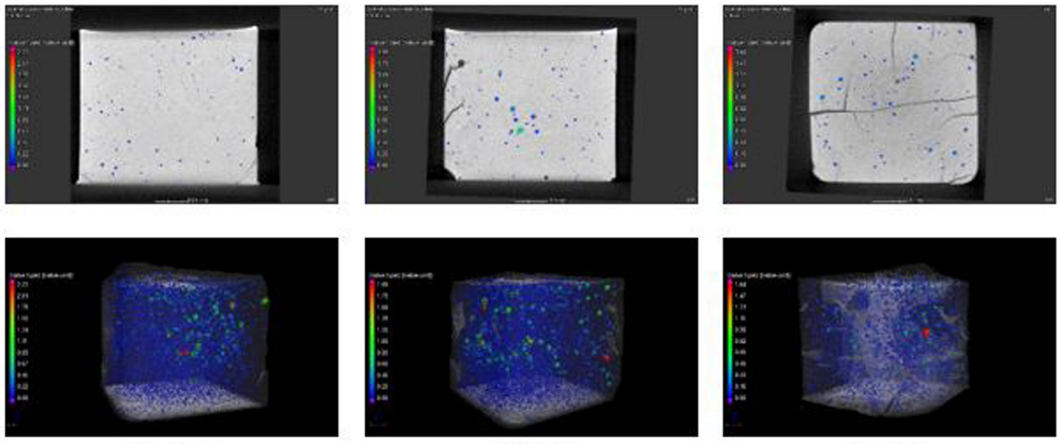

20±3°C 250°C 750°C

a)

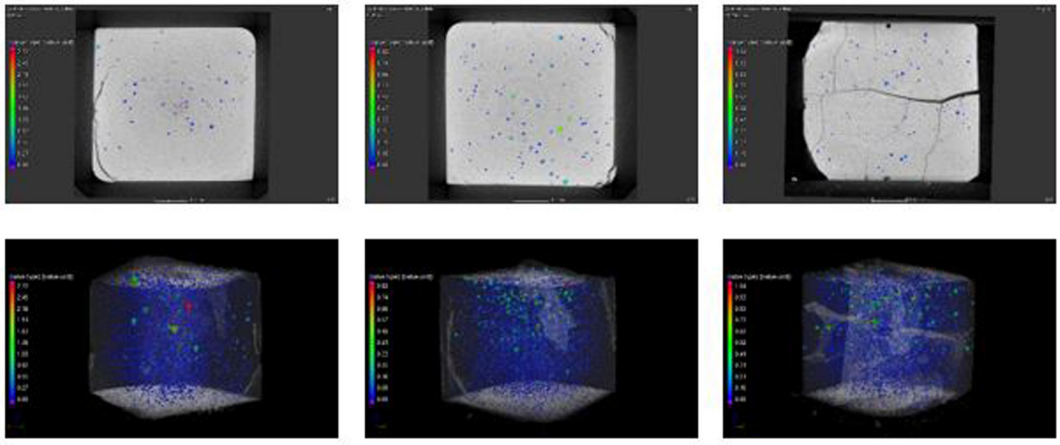

20±3°C 250°C 750°C

b)

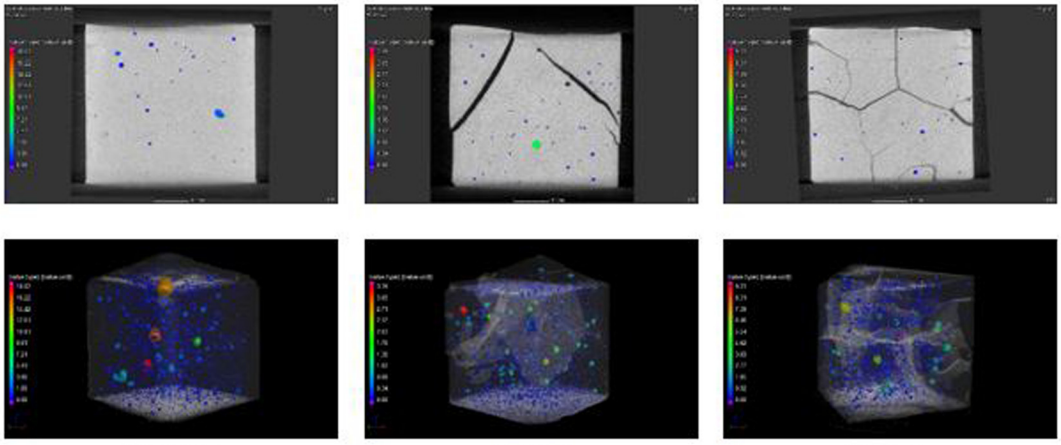

20±3°C 250°C 750°C

c)

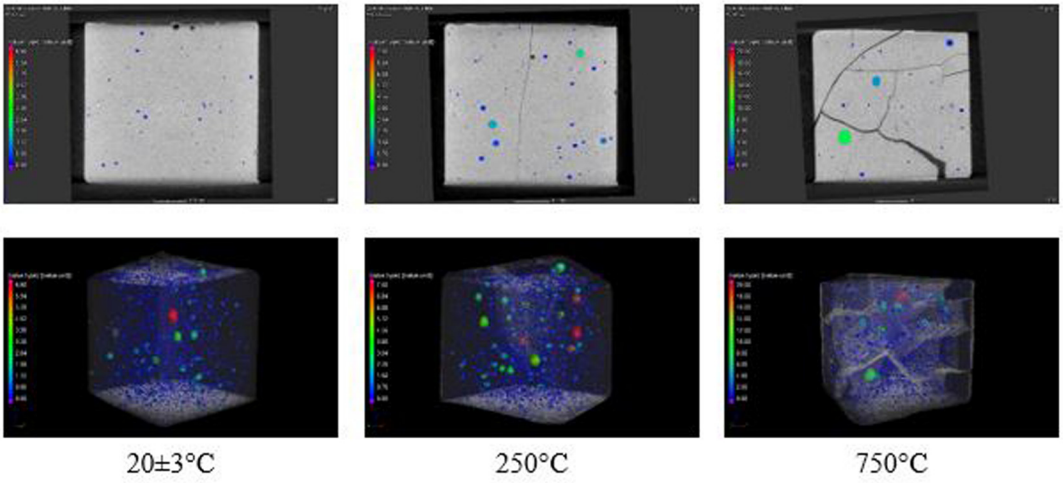

d)

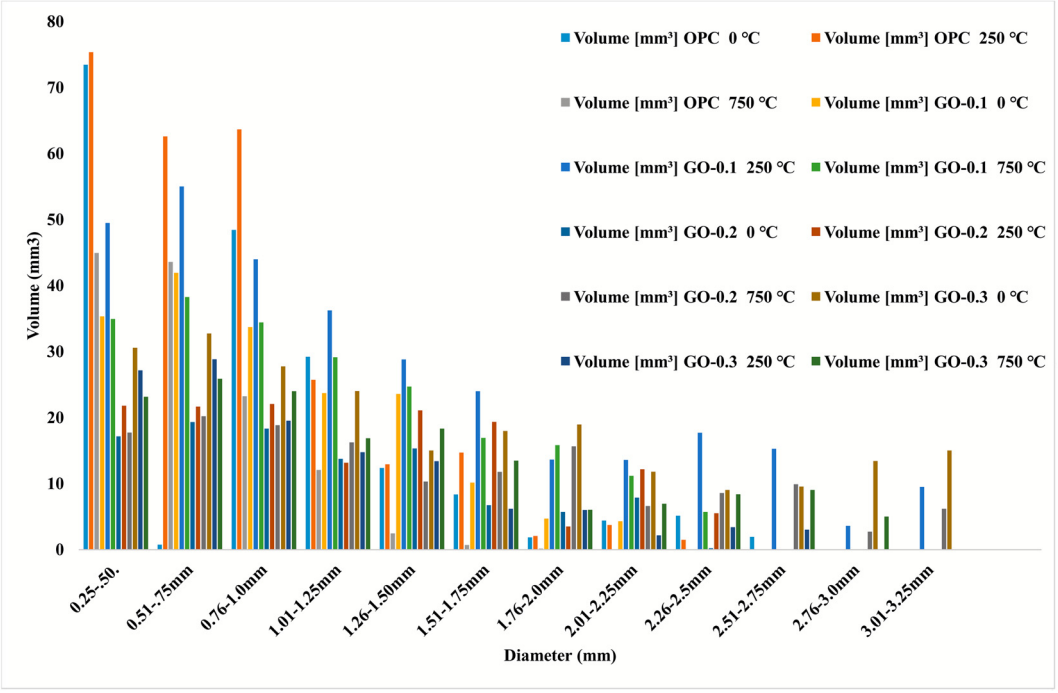

e)

Figure 9: Micro-CT analysis before and after thermal exposure: (a) OPC, (b) GO-0.1, (c) GO-0.2, (d) GO-0.3, and (e) porous void volumes by voids diameter sizes.

are consistent with the TG analysis (Section 3.2.2), which discovered that the presence of GO delayed thermal decomposition from 450 to 600°C. When the cement pastes were exposed to 600°C, their strength decreased significantly, with the samples retaining 80–92% of their initial strength. When the cement pastes were heated to 1,000°C, their strength decreased noticeably, with samples retaining 40–60% of their initial strength. After 500°C, with the total decomposition of C–S–H gel, the mechanical properties of the cement-based composites deteriorated, accompanied by a significant increase in disruptive cracks in the samples. The difference in the strength between unmodified and modified cement pastes also reduced. This observation is valid, because GO would burn after exposure to 600°C, as demonstrated by the TG results in Section 3.2.2. Furthermore, the ability to improve the compressive strength of samples at elevated temperatures decreased as the content of nanomaterials increased. After exposure at 500°C, a drastic reduction in

Table 3: Micro-CT data for material volume

	Data	20 ± 3°C	250°C	750°C
OPC	Material volume (mm³)	23180.52	23018.18	20263.54
	Defected volume (mm³)	273.56	260.14	145.98
GO-0.1	Material volume (mm³)	23995.16	24348.31	21957.21
	Defected volume (mm³)	189.13	329.4	288.28
GO-0.2	Material volume (mm³)	24700.54	24546.14	22244.33
	Defected volume (mm³)	118.05	213.93	165.57
GO-0.3	Material volume (mm³)	25004.97	24465.54	22508.38
	Defected volume (mm³)	241.13	147.6	208.74

the strengths of GO-0.2 and GO-0.3 specimens was observed. As a result, 0.1 wt% of GO was the optimum GO content for refining the microstructure after 28 days of curing; a higher GO content diminished the effect. Some studies used micro-CT to examine the microstructure of cement pastes after certain test temperatures to understand this phenomenon.

3.4 Micro-CT analysis and visual examination

Figure 9 and Table 3 demonstrate the micro-CT visuals of the specimens after heating to 20 ± 3, 250, and 750°C (above the ambient temperature). Micro-CT images were also used for qualitative and quantitative data for material volume and defected volume investigations. For the micro-CT evaluation, pores larger than 10 µm (the pixel size of the CT images) were considered. These pore sizes were considered to determine the defected volume and total material volume (Vc). The material volume refers to the volume of hydration product and aggregate volume that remains after heating the specimens, while defected volume refers to the volume of dehydration and dehydroxylation products that escape after the specimens are heated. Figure 9 demonstrates the variation in the number of deficiencies in the specimens with increasing temperature. In all the specimens, after exposure to 250°C, a subtle coarsening of the porous structure resulted in comparison with the unheated specimens. Changes in the microstructure of cement paste at this temperature are primarily associated with the release of water and initiation of the process of decomposition of hydration products [41,97]. This coarsens the pore structure as reported previously [94]. The porosity variations at this temperature are subtle, as observed in our study. Nonetheless, there was a discernible difference between the OPC specimen and GO-0.1, GO-0.2, and GO-0.3 specimens. Cracks were discovered in plain OPC specimens, but no visible cracks were found in the GO-0.1, GO-0.2, and GO-0.3 specimens with coarsened pores. The total material volume (Vc) of sample OPC at 0°C was 23180.52 mm^3, while the GO-0.1, GO-0.2, and GO-0.3 specimens' total volumes were 23995.16, 24700.54, and 25004.97 mm^3, respectively. Moreover, the defect volumes were 273.56, 189.13, 118.05, and 241.13 mm^3 for the OPC, GO-0.1, GO-0.2, and GO-0.3 specimens, respectively. Here, GO contained higher amounts of hydration products than OPC and the retainment of CH was also high. Additionally, the volume change ratio at 20 ± 3°C was expressed in percent for OPC, GO-0.1, GO-0.2, GO-0.3, respectively.

The microstructure of cement pastes deteriorated noticeably when exposed to 250°C. All specimens had discernible cracking patterns after being exposed to 250°C. These cracks and volume changes are primarily caused by C–S–H dehydration. The OPC specimen's volume change ratio was 1.13%, which was determined using the material volume (23018.18 mm^3) and defected volume (260.14 mm^3). However, the GO-0.1 specimen had 1.35% volume change ratio (material volume of 24348.31 mm^3 and defected volume of 329.4 mm^3). GO-0.1 had the least cracking followed by GO-0.2 and GO-0.3 (volume change ratios of 0.872 and 0.63%, respectively). Figure 9 verifies that using GO reduces cement paste cracking at this temperature. When the amount of GO in the specimens was increased, however, the opposite behaviors were observed. In Figure 9, the GO-0.2 and GO-0.3 specimens had larger and more cracks than the GO-0.1 specimens. In both specimens (GO-0.2 and GO-0.3), the volume change ratios were 0.872 and 0.63% at 250°C, respectively; this was smaller than the corresponding GO-0.1 value (1.35%). This means that the material volume of GO-0.2 and GO-0.3 is less stable than that of GO-0.1. The use of the appropriate amount of GO possibly made the C–S–H bond stronger leading to this effect. As shown in Figure 12, after exposure to 750°C, both the mechanical characteristics of specimens and the microstructure of cementitious

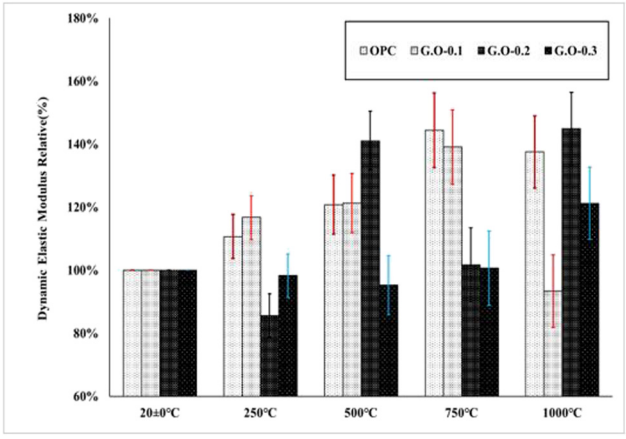

Figure 10: Dynamic elastic modulus relative (%) at different temperatures.

materials underwent degradation. Exposure to temperatures above 450°C resulted in the increased dissolution of the C–S–H phase and also the initiation of CH decomposition (400–550°C) [98,99]. The micro-CT study revealed that these phenomena contributed to a significant increase in cement matrix porosity along with micro-cracking. The total material volume of the OPC specimen was 20263.54 mm^3 at exposure to 750°C. The incorporation of 0.1, 0.2, and 0.3 wt% of GO resulted in a significant reduction in the cracking process. Here, the cracking is visible in Figure 9, and the changes in material volume when the cracks formed in the specimens are also mentioned. Furthermore, for GO-0.1, the single microcracks were wider and longer. In contrast, the specimens containing 0.2 and 0.3 wt% of GO were more prone to cracking than the OPC specimen or the specimens containing the optimal amount of GO (GO-0.1). The total material volume increased significantly for GO-0.1, GO-0.2, and GO-0.3. These findings are consistent with the compressive strength results presented in the previous section.

According to optical microscopy analysis, the favorable effects of GO incorporation, identified by micro-CT, can also be characterized on the macro-scale. However, only minor imperfections were ascertained in the specimens due to the limited changes in the microstructure after exposure to 250°C. As a result, the visual inspection included only the samples exposed to temperatures of 250 and 750°C. The highest deterioration rate was observed for the OPC

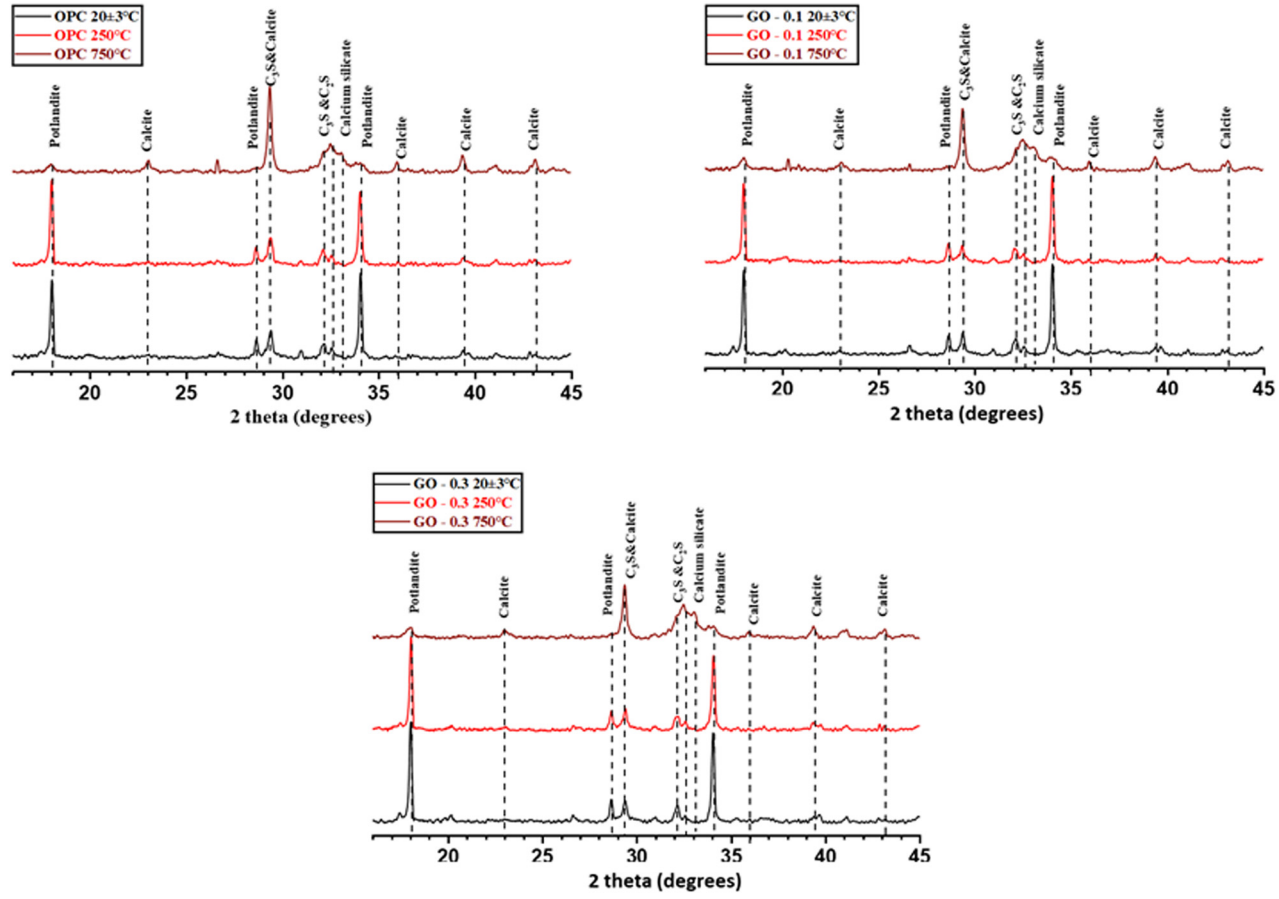

Figure 11: XRD patterns after thermal exposure.

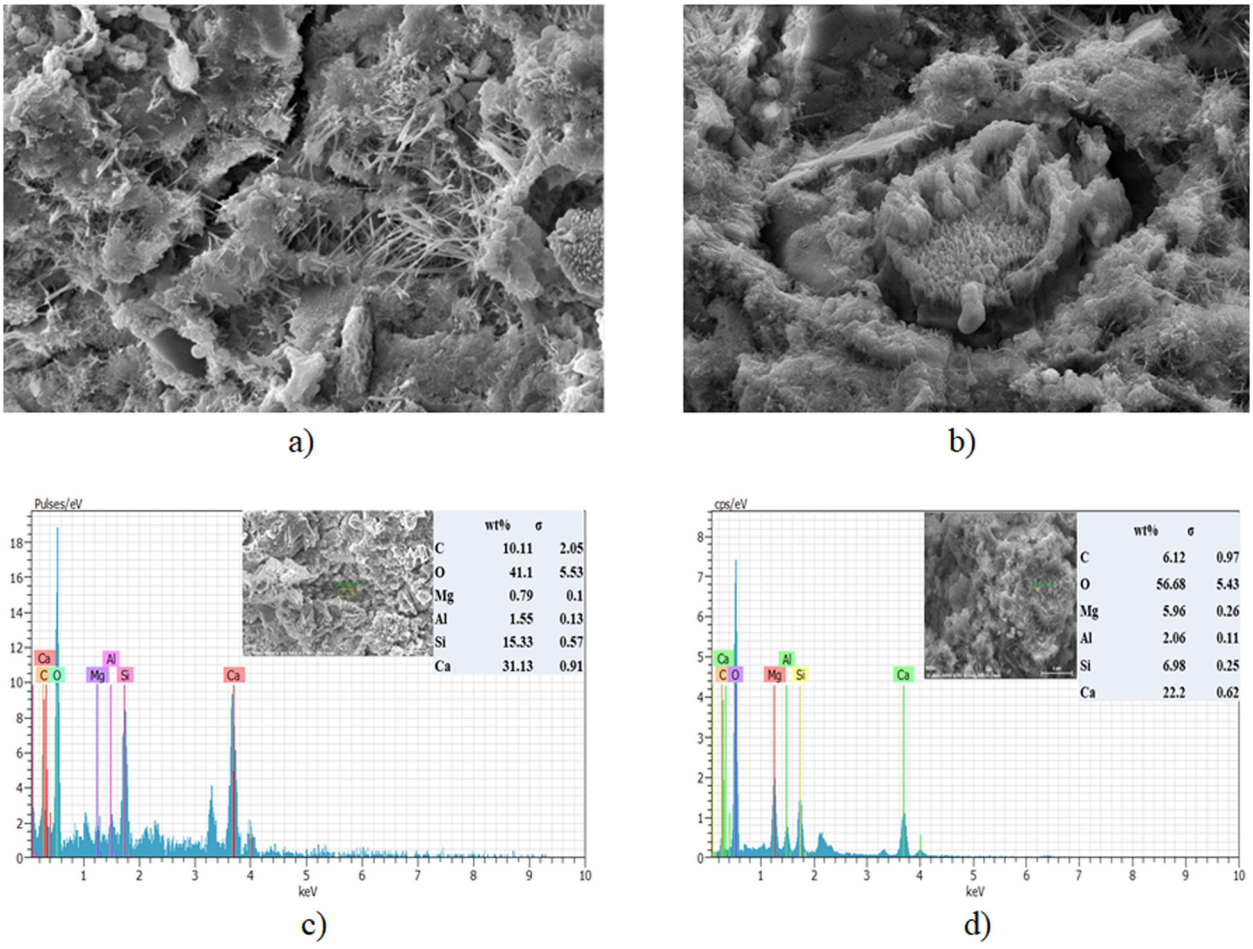

Figure 12: SEM and energy dispersive spectroscopy (EDS) of GO-0.1 and 0.2 at 28 days: (a) SEM GO-0.1, (b) SEM GO-0.2, (c) EDS GO-0.1, and (d) EDS GO-0.2.

specimen after exposure to 750°C, with GO-0.1, GO-0.2, and GO-0.3 exhibiting a comparable number of surface cracks. Furthermore, after exposure to 750°C, both the mechanical characteristics of specimens and the microstructure of cementitious materials underwent degradation. A visual inspection confirmed the findings of the micro-CT analysis.

Cluster formation results when the quantity of GO surpasses the optimum amount, leading to an increase in cement matrix porosity and a consequent reduction in strength. The effect was not pronounced in specimens containing 0.2 wt% of GO; however, the incorporation of 0.3 wt% of GO resulted in strength and microstructure degradation as the temperature increased.

As a result, incorporating the optimum amount of GO is critical for providing adequate thermal tolerance. Microstructural and mechanical effectiveness of the specimens can be expected to improve when appropriate amount of GO is incorporated. GO facilitates better mechanical characteristics in the cement composites due to its enhanced binding capacity with cement matrices and nanoparticles and its higher thermal resistance, which leads to a higher strength in the unheated state and during exposure to temperatures of up to 750°C (compared with that of OPC).

3.5 Dynamic modulus of elasticity

Table 4 summarizes the elastic modulus from the dynamic modulus of elasticity measurement by the resonance vibration equipment. In general, the stiffness and volume of the components have a significant influence on the elastic modulus of composites. Given that the GO weight fraction in cement paste is only 0.05%, it is not surprising that the elastic modulus of the GO cement composite is close to that of the cement paste. A minor increase in the elastic modulus (from 3.48 to 3.70 GPa) could be attributed to a reduction in the number of original shrinkage cracks due to the effect of GO. Here, the dynamic modulus of elasticity range is 22.08–34.19 GPa based on the considered

Table 4: Dynamic modulus of elasticity of the specimens

Type	Dynamic modulus of elasticity based on temperature (GPa)			
	250°C	500°C	750°C	1,000°C
OPC	26.06	31.51	33.89	32.47
GO-0.1	27.57	30.39	32.75	28.62
GO-0.2	24.29	34.19	23.93	32.32
GO-0.3	22.08	23.11	23.82	33.68

exposure temperature values (250, 500, 750, and 1,000°C). Decarbonation in GO-0.2 at ~700°C could have caused the decrease in the dynamic modulus of elasticity of the GO-0.2 specimen at 750°C. The dynamic modulus of elasticity of the specimens at different temperatures is compared in Figure 10. A higher dynamic elastic modulus relative (%) suggests that the concrete can withstand higher loads based on its strength and brittleness properties.

3.6 XRD analysis after thermal exposure

After heating, all experimental samples were stored in a dry state for more than 7 days before performing the XRD experiments. The C3S peak in the G-0.1 sample decreased when the temperature reached 250°C indicating that the hydration continued. The same effect was responsible for the compressive strength enhancement. There was no significant difference in the crystal plane peaks of hydration products of the OPC sample and the G-0.3 sample at 0 and 250°C, and the C3S clinker peak of the G-0.1 sample was reduced. This indicated the progression of clinker hydration, possibly leading to an increase in the compressive strength. Furthermore, after heating to 750°C, the crystal plane peak disappeared in all the samples due to portlandite dehydration, and the crystal plane peak of calcium silicate produced by the decomposition of C–S–H gel was increased. After 7 days of temperature rise, all specimens were stored in dry condition, and the XRD experiment was performed to recover calcite from the initial temperature product. In comparison with OPC, the GO-incorporated sample had a lower peak of calcite crystal plane; this had an impact on the recovery process (Figure 11).

3.7 SEM and EDS

Scanning electron microscopy (SEM) imaging was used to investigate the behavior of GO 0.1 and 0.2% on the cement hydration crystal. The microstructures of the hydrated cement mixed with GO (0.1 and 0.2%) at 28 days are represented in the SEM and EDS results as shown in Figure 12. The SEM image of the microstructure of cement paste after 28 days demonstrates that the GO content had a dominant effect on the intensity of flower-shaped needle-like crystal-like structures. The products of cement hydration have a flower-shaped 5 content of 0.1 and 0.2% by weight of cement. During the 28-day curing period, the flower-shaped needle-like crystalline form becomes thinner and denser as the GO content increases from 0.1 to 0.2%. The $CaCO_3$ crystal distribution in hydrated cement composites would be identified by inspecting the $CaCO_3$ crystal in the entire SEM using EDS.

4 Conclusion

An extensive experimental investigation was performed to characterize the mechanical properties of cement composites to investigate the mechanism of GO in improving the properties of cement composites and the microstructure of GO cement composites. Based on the results obtained in this study, the following conclusions were derived:

1) For a constant w/c ratio, the compressive strength of cement pastes with 0.1, 0.2, and 0.3 wt% of GO was higher than that of the OPC paste. The porosity was analyzed to understand the effect of nanoscale micro-cracking on the mechanical properties. Among all the samples tested after 28 and 56 days of curing, GO-0.1 was optimal for compressive strength enhancement.
2) Thermal exposure resulted in additional hydration of anhydrous cement grains; this increased the compressive strength of the GO-0.1 sample at 250°C compared with the unheated sample. However, after exposure to temperatures above 500°C, the compressive strengths of GO-0.2 and GO-0.3 samples deteriorated compared with that of the OPC sample, while the compressive strength of the GO-0.1 sample was higher than that of the OPC sample. This resulted from the chemical compositional effect.
3) The incorporation of the optimal amount of GO resulted in the reduction of cracking of specimens under the tested temperatures of up to 500°C. However, the excessive agglomeration of GO nanosheets reduced the thermal resistance of cement paste resulting in lower strength values and increased micro-cracking.

4) The measured dynamic modulus of elasticity and XRD analysis after thermal exposure demonstrates the enhancement in mechanical characteristics of the GO cement composite. The results of the study can be used to arrive at the optimum content of GO for the desired mechanical characteristics of the cement nanocomposites.

Investigations with GO revealed that it has good reinforcing and microstructural properties due to its active functional groups, as well as a much higher specific surface area than 0-D nanoparticles. At the molecular level, GO has been shown to influence cement hydration properties. The direct mixing of GO in cement improves the mechanical properties of the resulting composites due to changes in pore size distribution, the formation of gel materials in the pores, and the resulting ability to effectively inhibit ion ingress. The nano-reinforcing and water-dispersion properties of GO could be investigated further in order to develop self-healing concrete and other self-repairing materials. When compared to cement and other cement supplementary nanomaterials, the production of GO is highly environmentally friendly. As a result, an in-depth life-cycle cost assessment and carbon footprint analysis of GO–cement-based composite systems should be performed. Advances in GO production and GO–cement composite materials may increase construction efficiency, while reducing the overall carbon into the environment.

Funding information: This research was funded by the National Research Foundation (NRF) of Korea and grant No. NRF-2019R1A6A3A01096309 and NRF-2020R1A2C3009894

Author contributions: All authors have accepted responsibility for the entire content of this manuscript and approved its submission.

Conflict of interest: The authors state no conflict of interest.

References

[1] Balaguru P, Chong K. Nanotechnology and concrete: research opportunities. Proceedings of ACI session on nanotechnology of concrete: recent developments and future perspectives. Denver, USA; November, 2006. p. 15–28.

[2] Kumar A, Kumar S, Mukhopadhyay NK, Yadav A, Kumar V, Winczek J. Effect of variation of SiC reinforcement on wear behaviour of AZ91 alloy composites. Materials. 2021;14(4):990.

[3] Abebe Emiru A, Sinha DK, Kumar A, Yadav A. Fabrication and characterization of hybrid aluminium (Al6061) metal matrix composite reinforced with SiC, B_4C and MoS_2 via stir casting. Int J Metalcast. 2022;1–12. doi: 10.1007/s40962-022-00800-1.

[4] Ali KSA, Mohanavel V, Vendan SA, Ravichandran M, Yadav A, Gucwa M, et al. Mechanical and microstructural characterization of friction stir welded SiC and B_4C reinforced aluminium alloy AA6061 metal matrix composites. Materials. 2021;14(11):3110.

[5] Li Q, He C, Zhou H, Xie Z, Li D. Effects of polycarboxylate superplasticizer-modified graphene oxide on hydration characteristics and mechanical behavior of cement. Constr Build Mater. 2021;272:121904.

[6] Jiang Z, Sevim O, Ozbulut OE. Mechanical properties of graphene nanoplatelets-reinforced concrete prepared with different dispersion techniques. Constr Build Mater. 2021;303:124472.

[7] Mowlaei R, Lin J, de Souza FB, Fouladi A, Korayem AH, Shamsaei E, et al. The effects of graphene oxide–silica nanohybrids on the workability, hydration, and mechanical properties of Portland cement paste. Constr Build Mater. 2021;266:121016.

[8] Chuah S, Pan Z, Sanjayan JG, Wang CM, Duan WH. Nano reinforced cement and concrete composites and new perspective from graphene oxide. Constr Build Mater. 2014;73:113–24. doi: 10.1016/j.conbuildmat.2014.09.040.

[9] Pan Z, He L, Qiu L, Korayem AH, Li G, Zhu JW, et al. Mechanical properties and microstructure of a graphene oxide–cement composite. Cement Concr Compos. 2015;58:140–7. doi: 10.1016/j.cemconcomp.2015.02.001.

[10] Brodie BC. XIII. On the atomic weight of graphite. Philos Trans R Soc London. 1859;149:249–59. doi: 10.1098/rstl.1859.0013.

[11] Zeng H, Lai Y, Qu S, Yu F. Effect of graphene oxide on permeability of cement materials: an experimental and theoretical perspective. J Build Eng. 2021;41:102326.

[12] Kumar HV, Woltornist SJ, Adamson DH. Fractionation and characterization of graphene oxide by oxidation extent through emulsion stabilization. Carbon. 2016;98:491–5. doi: 10.1016/j.carbon.2015.10.083.

[13] Tong T, Fan Z, Liu Q, Wang S, Tan S, Yu Q. Investigation of the effects of graphene and graphene oxide nanoplatelets on the micro-and macro-properties of cementitious materials. Constr Build Mater. 2016;106:102–14. doi: 10.1016/j.conbuildmat.2015.12.092.

[14] Chuah S, Li W, Chen SJ, Sanjayan JG, Duan WH. Investigation on dispersion of graphene oxide in cement composite using different surfactant treatments. Constr Build Mater. 2018;161:519–27. doi: 10.1016/j.conbuildmat.2017.11.154.

[15] Liu C, Huang X, Wu YY, Deng X, Zheng Z, Xu Z, et al. Advance on the dispersion treatment of graphene oxide and the graphene oxide modified cement-based materials. Nanotechnol Rev. 2021;10(1):34–49.

[16] Suo Y, Guo R, Xia H, Yang Y, Zhou B, Zhao Z. A review of graphene oxide/cement composites: performance, functionality, mechanisms, and prospects. J Build Eng. 2022;53:104502.

[17] Li X, Lu Z, Chuah S, Li W, Liu Y, Duan WH, et al. Effects of graphene oxide aggregates on hydration degree, sorptivity, and tensile splitting strength of cement paste. Compos Appl

Sci Manuf. 2017;100:1–8. doi: 10.1016/j.compositesa.2017.05.002.
[18] Dikin DA, Stankovich S, Zimney EJ, Piner RD, Dommett GH, Evmenenko G, et al. Preparation and characterization of graphene oxide paper. Nature. 2007;448(7152):457–60. doi: 10.1038/nature06016.
[19] Li X, Korayem AH, Li C, Liu Y, He H, Sanjayan JG, et al. Incorporation of graphene oxide and silica fume into cement paste: a study of dispersion and compressive strength. Constr Build Mater. 2016;123:327–35. doi: 10.1016/j.conbuildmat.2016.07.022.
[20] Li GY, Wang PM, Zhao X. Mechanical behavior and microstructure of cement composites incorporating surface-treated multi-walled carbon nanotubes. Carbon. 2005;43(6):1239–45. doi: 10.1016/j.carbon.2004.12.017.
[21] Shang Y, Zhang D, Yang C, Liu Y, Liu Y. Effect of graphene oxide on the rheological properties of cement pastes. Constr Build Mater. 2015;96:20–8. doi: 10.1016/j.conbuildmat.2015.07.181.
[22] Gong K, Pan Z, Korayem AH, Qiu L, Li D, Collins F, et al. Reinforcing effects of graphene oxide on portland cement paste. J Mater Civ Eng. 2015;27(2):A4014010. doi: 10.1061/(asce)mt.1943-5533.0001125.
[23] Zhu Y, Murali S, Cai W, Li X, Suk JW, Potts JR, et al. Graphene and graphene oxide: synthesis, properties, and applications. Adv Mater. 2010;22(35):3906–24. doi: 10.1002/adma.201001068.
[24] Lv S, Liu J, Sun T, Ma Y, Zhou Q. Effect of GO nanosheets on shapes of cement hydration crystals and their formation process. Constr Build Mater. 2014;64:231–9. doi: 10.1016/j.conbuildmat.2014.04.061.
[25] Lv S, Ma Y, Qiu C, Sun T, Liu J, Zhou Q. Effect of graphene oxide nanosheets of microstructure and mechanical properties of cement composites. Constr Build Mater. 2013;49:121–7. doi: 10.1016/j.conbuildmat.2013.08.022.
[26] Liu C, Huang X, Wu YY, Deng X, Zheng Z. The effect of graphene oxide on the mechanical properties, impermeability and corrosion resistance of cement mortar containing mineral admixtures. Constr Build Mater. 2021;288:123059.
[27] Indukuri CSR, Nerella R. Enhanced transport properties of graphene oxide based cement composite material. J Build Eng. 2021;37:102174.
[28] Chen Y, Li X, Dong B, Du H, Yan R, Wang L. High-temperature properties of cement paste with graphene oxide agglomerates. Constr Build Mater. 2022;320:126286. doi: 10.1016/j.conbuildmat.2021.126286.
[29] Hager I. Behaviour of cement concrete at high temperature. Bull Pol Acad Sci Tech Sci. 2013;61(1):145–54. doi: 10.2478/bpasts-2013-0013.
[30] Fernandes B, Gil AM, Bolina FL, Tutikian BF. Microstructure of concrete subjected to elevated temperatures: physico-chemical changes and analysis techniques. IBRACON Struct Mater J. 2017;10:838–63. doi: 10.1590/S1983-41952017000400004.
[31] Sikora P, Abd Elrahman M, Chung SY, Cendrowski K, Mijowska E, Stephan D. Mechanical and microstructural properties of cement pastes containing carbon nanotubes and carbon nanotube–silica core–shell structures, exposed to elevated temperature. Cement Concr Compos. 2019;95:193–204. doi: 10.1016/j.cemconcomp.2018.11.006.
[32] Khoury GA. Effect of fire on concrete and concrete structures. Prog Struct Eng Mater. 2000;2(4):429–47. doi: 10.1002/pse.51.
[33] Kodur V. Properties of concrete at elevated temperatures. ISRN. 2014;2014:1–15. doi: 10.1155/2014/468510.
[34] Ma Q, Guo R, Zhao Z, Lin Z, He K. Mechanical properties of concrete at high temperature – a review. Constr Build Mater. 2015;93:371–83. doi: 10.1016/j.conbuildmat.2015.05.131.
[35] Haneefa KM, Santhanam M, Parida FC. Review of concrete performance at elevated temperature and hot sodium exposure applications in nuclear industry. Nucl Eng Des. 2013;258:76–88. doi: 10.1016/j.nucengdes.2013.01.018.
[36] El-Gamal SM, Abo-El-Enein SA, El-Hosiny FI, Amin MS, Ramadan M. Thermal resistance, microstructure and mechanical properties of type I Portland cement pastes containing low-cost nanoparticles. J Therm Anal Calorim. 2018;131(2):949–68. doi: https://doi.org/10.1007/s10973-017-6629-1.
[37] Heikal M, Ismail MN, Ibrahim NS. Physico-mechanical, microstructure characteristics and fire resistance of cement pastes containing Al_2O_3 nano-particles. Constr Build Mater. 2015;91:232–42. doi: 10.1016/j.conbuildmat.2015.05.036.
[38] Horszczaruk E, Sikora P, Cendrowski K, Mijowska E. The effect of elevated temperature on the properties of cement mortars containing nanosilica and heavyweight aggregates. Constr Build Mater. 2017;137:420–31. doi: 10.1016/j.conbuildmat.2017.02.003.
[39] Irshidat MR, Al-Saleh MH. Thermal performance and fire resistance of nanoclay modified cementitious materials. Constr Build Mater. 2018;159:213–9. doi: 10.1016/j.conbuildmat.2017.10.127.
[40] Lim S, Mondal P. Effects of nanosilica addition on increased thermal stability of cement-based composite. ACI Mater J. 2015;112(2):305–15. doi: 10.3342/kjorl-hns.2015.58.5.305.
[41] Marushchak U, Sanytsky M, Olevych Y. Effects of elevated temperatures on the properties of nanomodified rapid hardening concretes. MATEC Web Conf. 2017;116(5):1008. doi: 10.1051/matecconf/201711601008.
[42] Wang WC. Compressive strength and thermal conductivity of concrete with nanoclay under various high-temperatures. Constr Build Mater. 2017;147:305–11. doi: 10.1016/j.conbuildmat.2017.04.141.
[43] Mohammed A, Sanjayan JG, Nazari A, Al-Saadi NT. Effects of graphene oxide in enhancing the performance of concrete exposed to high-temperature. Aust J Civ Eng. 2017;15(1):61–71. doi: 10.1080/14488353.2017.1372849.
[44] Zhang LW, Kai MF, Liew KM. Evaluation of microstructure and mechanical performance of CNT-reinforced cementitious composites at elevated temperatures. Compos Part A. 2017;95:286–93. doi: 10.1016/j.compositesa.2017.02.001.
[45] Chu HY, Jiang JY, Sun W, Zhang M. Mechanical and thermal properties of graphene sulfonate nanosheet reinforced sacrificial concrete at elevated temperatures. Constr Build Mater. 2017;153:682–94. doi: 10.1016/j.conbuildmat.2017.07.157.
[46] Amin MS, El-Gamal SM, Hashem FS. Fire resistance and mechanical properties of carbon nanotubes–clay bricks wastes (Homra) composites cement. Constr Build Mater. 2015;98:237–49. doi: 10.1016/j.conbuildmat.2015.08.074.

[47] Mohammed A, Sanjayan JG, Duan WH, Nazari A. Incorporating graphene oxide in cement composites: a study of transport properties. Constr Build Mater. 2015;84:341–7. doi: 10.1016/j.conbuildmat.2015.01.083.
[48] Wang Q, Wang J, Lu CX, Liu BW, Zhang K, Li CZ. Influence of graphene oxide additions on the microstructure and mechanical strength of cement. New Carbon Mater. 2015;30(4):349–56. doi: 10.1016/S1872-5805(15)60194-9.
[49] Chakraborty S, Kundu SP, Roy A, Adhikari B, Majumder SB. Effect of jute as fiber reinforcement controlling the hydration characteristics of cement matrix. Ind Eng Chem Res. 2013;52(3):1252–60. doi: 10.1021/ie300607r.
[50] Zhai S, Pang B, Liu G, Zhang Y, Xu K, She W, et al. Investigation 2pt?>on preparation and multifunctionality of reduced graphene oxide cement mortar. Constr Build Mater. 2021;275:122119.
[51] Lu Z, Hou D, Meng L, Sun G, Lu C, Li Z. Mechanism of cement paste reinforced by graphene oxide/carbon nanotubes composites with enhanced mechanical properties. RSC Adv. 2015;5(122):100598–605. doi: 10.1039/c5ra18602a.
[52] Stankovich S, Dikin DA, Dommett GH, Kohlhaas KM, Zimney EJ, Stach EA, et al. Graphene-based composite materials. Nature. 2006;442(7100):282–6.
[53] Stankovich S, Piner RD, Chen X, Wu N, Nguyen ST, Ruoff RS. Stable aqueous dispersions of graphitic nano platelets via the reduction of exfoliated graphite oxide in the presence of poly (sodium 4-styrene suffocate). J Mater Chem. 2006;16(2):155–8.
[54] Zhu Y, Murali S, Cai W, Li X, Suk JW, Potts JR, et al. Graphene and graphene oxide: synthesis, properties, and applications. Adv Mater. 2010;22(35):3906–24.
[55] Alkhateb H, Alostaz A, Cheng AHD, Li X. Materials genome for graphene–cement nanocomposites. J Nanomech Micromech. 2013;3:67–77.
[56] Fan Z. Investigation on properties of cementitious materials reinforced by graphene. Pittsburgh: University of Pittsburgh; 2014.
[57] Babak F, Abolfazl H, Alimorad R, Parviz G. Preparation and mechanical properties of graphene oxide: cement nanocomposites. Sci World J. 2014;1:1–10.
[58] Pellenq RJM, Van Damme H. Why does concrete set? The nature of cohesion forces in hardened cement-based materials. MRS Bull. 2011;29(5):319–23.
[59] Liu Y, Jia M, Song C, Lu S, Wang H, Zhang G, et al. Enhancing ultra-early strength of sulphoaluminate cement-based materials by incorporating graphene oxide. Nanotechnol Rev. 2020;9(1):17–27.
[60] Wang L, Li Q, Song J, Liu S. Effect of graphene oxide on early hydration and compressive strength of Portland cementcopper tailing powder composite binder. Powder Technol. 2021;386:428–36.
[61] Kong D, Huang S, Corr D, Yang Y Shah SP. Whether do nanoparticles act as nucleation sites for C–S–H gel growth during cement hydration. Cem Concr Compos. 2018;87:98–109.
[62] Neville AM. Properties of concrete. Chichester: Wiley; 2012.
[63] Nathan B, Chaurand P, Vicente J, Borschneck D, Levard C, Aguerre-Chariol O, et al. Micro- and nano-X-ray computed-tomography: a step forward in the characterization of the pore network of a leached cement paste. Cement Concr Res. 2015;67:138–47.
[64] Chung S-Y, Abd Elrahman M, Sikora P, Rucinska T, Horszczaruk E, Stephan D. Evaluation of the effects of crushed and expanded waste glass aggregates on the material properties of lightweight concrete using image-based approaches. Materials. 2017;10:1354.
[65] Zhang M. Pore-scale modelling of relative permeability of cementitious materials using X-ray computed microtomography images. Cement Concr Res. 2017;95:18–29.
[66] Lu H, Alymov E, Shah S, Peterson K. Measurement of air void system in lightweight concrete by X-ray computed tomography. Constr Build Mater. 2017;152:467–83.
[67] Gastaldi D, Canonico F, Capelli L, Boccaleri E, Milanesio M, Palin L, et al. In situ tomographic investigation on the early hydration behaviors of cementing systems. Constr Build Mater. 2012;29:284–90.
[68] Parisatto M, Dalconi MC, Valentini L, Artioli G, Rack A, Tucoulou R, et al. Examining microstructural evolution of Portland cements by in-situ synchrotron micro-tomography. J Mater Sci. 2015;50:1805–17.
[69] Huang Y, Yan D, Yang Z, Liu G. 2D and 3D homogenization and fracture analysis of concrete based on in-situ X-ray Computed Tomography images and Monte Carlo simulations. Eng Fract Mech. 2016;163:37–54.
[70] Huang Y, Yang Z, Ren W, Liu G, Zhang C. 3D meso-scale fracture modelling and validation of concrete based on in-situ X-ray Computed Tomography images using damage plasticity model. Int J Solid Struct. 2015;67–68:340–52.
[71] Yang Z, Ren W, Sharma R, McDonald S, Mostafavi M, Vertyagina Y, et al. In situ X-ray computed tomography characterisation of 3D fracture evolution and image-based numerical homogenisation of concrete. Cement Concr Compos. 2017;75:74–83.
[72] Yang HB, Cui HZ, Tang WC, Li ZJ, Han NX, Xing F. A critical review on research progress of graphene/cement based composites. Compos Part A. 2017;102:273–96.
[73] Wang Q, Wang J, Lv CX, Cui XY, Li SY, Wang X. Rheological behavior of fresh cement pastes with a graphene oxide additive. New Carbon Mater. 2016;31(6):574–84.
[74] Zheng QF, Han BG, Cui X, Yu X, Ou JP. Graphene-engineered cementitious composites: small makes a big impact. Nanomater Nanotechnol. 2017;7:1–18.
[75] Li ZY, Liu YM, Li WG, Li CY, Sanjayan JG, Duan WH, et al. Effects of graphene oxide agglomerates on workability, hydration, microstructure and compressive strength of cement paste. Constr Build Mater. 2017;145:402–10.
[76] Lu ZY, Li ZY, Hanif A, Chen BM, Parthasarathy P, Yu JG, et al. Early-age interaction mechanism between the graphene oxide and cement hydrates. Constr Build Mater. 2017;152:232–9.
[77] Wang M, Wang RM, Yao H, Wang ZJ. Adsorption characteristics of graphene oxide nanosheets on cement. RSC Adv. 2016;6:63365–72.
[78] Horszczaruk E, Mijowska E, Kalenczuk RJ, Aleksandrzak M, Mijowska S. Nanocomposite of cement/graphene oxide – impact on hydration kinetics and Young' s modulus. Const Build Mater. 2015;78:234–42.
[79] Long WJ, Ye TH, Gu YC, Li HD, Xing F. Inhibited effect of graphene oxide on calcium leaching of cement pastes. Constr Build Mater. 2019;202:177–88.
[80] Long WJ, Wei JJ, Xing F, Khayat KH. Enhanced dynamic mechanical properties of cement paste modified with

graphene oxide nanosheets and its reinforcing mechanism. Cem Concr Compos. 2018;93:127–39.
[81] Qin H, Wei W, Hu YH. Synergistic effect of graphene-oxide-doping and microwave-curing on mechanical strength of cement. J Phys Chem Solids. 2017;103:67–72.
[82] Sharma S, Kothiyal NC. Influence of graphene oxide as dispersed phase in cement mortar matrix in defining the crystal patterns of cement hydrates and its effect on mechanical, microstructural and crystallization properties. RSC Adv. 2015;5:52642–57.
[83] Lin CQ, Wei W, Hu YH. Catalytic behavior of graphene oxide for cement hydration process. J Phys Chem Solids. 2016;89:128–33.
[84] Qureshi TS, Panesar DK. Impact of graphene oxide and highly reduced graphene oxide on cement based composites. Constr Build Mater. 2019;206:71–83.
[85] Zhao L, Guo XL, Liu YY, Ge C, Guo LP, Shu X, et al. Synergistic effects of silica nanoparticles/polycarboxylate superplasticizer modified graphene oxide on mechanical behavior and hydration process of cement composites. RSC Adv. 2017;7:16688–702.
[86] Mavropoulou N, Katsiotis N, Giannakopoulos J, Koutsodontis K, Papageorgiou D, Chaniotakis E, et al. Durability evaluation of cement exposed to combined action of chloride and sulphate ions at elevated temperature: the role of limestone filler. Constr Build Mater. 2016;124:558–65.
[87] Huang HL, Qian CX, Zhao F, Qu J, Guo JQ, Danzinger M. Improvement on microstructure of concrete by polycarboxylate superplasticizer (PCE) and its influence on durability of concrete. Constr Build Mater. 2016;110:293–9.
[88] Devi SC, Khan RA. Effect of graphene oxide on mechanical and durability performance of concrete. J Build Eng. 2020;27:101007.
[89] Mohsen MO, Taha R, Abu Taqa A, Shaat A. Optimum carbon nanotubes' content for improving flexural and compressive strength of cement paste. Constr Build Mater. 2017;150:395–403.
[90] Lu L, Ouyang D, Xu W. Mechanical properties and durability of ultra high strength concrete incorporating multi-walled carbon nanotubes. Materials. 2016;9(6):419.
[91] Gholampour A, Kiamahalleh V, Tran M, Ozbakkaloglu DNT, Losic D. From graphene oxide to reduced graphene oxide: impact on the physiochemical and mechanical properties of graphene–cement composites. ACS Appl Mater Interfaces. 2017;9(49):43275–86.
[92] Lin Y, Du H. Graphene reinforced cement composites: a review. Constr Build Mater. 2020;265:120312.
[93] Heikal M, Ali AI, Ismail MN, Awad S, Ibrahim NS. Behavior of composite cement pastes containing silica nano-particles at elevated temperature. Constr Build Mater. 2014;70:339–50.
[94] Demirel B, Keleştemur O. Effect of elevated temperature on the mechanical properties of concrete produced with finely ground pumice and silica fume. Fire Saf J. 2010;45:385–91.
[95] Heikal M. Characteristics, textural properties and fire resistance of cement pastes containing Fe_2O_3 nano-particles. J Therm Anal Calorim. 2016;126:1077–87.
[96] Kang S-M, Na S-H, Kim K-N, Song M-S. Pore structure changes in hardened cement paste exposed to elevated temperature. J Kor Chem Soc. 2015;52(1):48–55.
[97] Hachemi S. Performance of concrete containing crushed brick aggregate exposed to different fire temperatures. Eur J Environ Civ Eng. 2015;19(7):805–24.
[98] Mendes A, Sanjayan JG, Gates WP, Collins F. The influence of water absorption and porosity on the deterioration of cement paste and concrete exposed to elevated temperatures, as in a fire event. Cement Concr Compos. 2012;34:1067–74.
[99] Heo Y, Lee G, Lee G. Effect of elevated temperatures on chemical properties, microstructure and carbonation of cement paste. J Ceram Process Res. 2016;17(6):648–52.